AIChE

A Mechanistic Model for the Water-Gas Shift Reaction over Noble Metal Substituted Ceria

Parag A. Deshpande
Dept. of Chemical Engineering, Indian Institute of Science, Bangalore 560012, India

M. S. Hegde
Solid State and Structural Chemistry Unit, Indian Institute of Science, Bangalore 560012, India

Giridhar Madras
Dept. of Chemical Engineering, Indian Institute of Science, Bangalore 560012, India
Solid State and Structural Chemistry Unit, Indian Institute of Science, Bangalore 560012, India

DOI 10.1002/aic.12062
Published online October 22, 2009 in Wiley InterScience (www.interscience.wiley.com).

The water-gas shift (WGS) reaction was carried out in the presence of Pd and Pt substituted nanocrystalline ceria catalysts synthesized by solution combustion technique. The catalysts were characterized by powder XRD and XPS. The noble metals were found to be present in ionic form substituted for the cerium atoms. The catalysts showed high activity for the WGS reaction with high conversions below 250°C. The products of reaction were only carbon dioxide and hydrogen, and no hydrocarbons were observed even in trace quantities. The reactions were carried out with different amounts of noble metal ion substitution and 2% Pt substituted ceria was found to be the best catalyst. The various possible mechanisms for the reaction were proposed and tested for their consistency with experimental data. The dual site mechanism best described the kinetics of the reaction and the corresponding rate parameters were obtained. © 2009 American Institute of Chemical Engineers *AIChE J,* 56: 1315–1324, 2010
Keywords: water-gas shift reaction, solution combustion technique, hydrogen production, reaction mechanisms

Introduction

Fuel cells are the energy devices in which direct conversion of chemical energy into electrical energy takes place without the involvement of an intermediate thermal cycle. However, the availability of cleaner and cheaper hydrogen still remains as a problem. To have low-operation temperatures of the fuel cell, hydrogen of very high purity is required.[1] In the fuel cells utilizing polymer electrolytes, the platinum electrode is highly prone to poisoning[2] by CO. It has been reported that in the feed with 1–10% CO impurity, adsorption of CO on the Pt electrode takes place irreversibly at low enough temperatures (80°C) and the electrochemical reactions are affected by this phenomenon.[3–5] Therefore, the concentration levels of CO in the H_2 feed stream are required to be less than 10–20 ppm.[4,6] Similarly, in case of direct methanol fuel cells, the presence of even traces of CO is highly detrimental for the electrodes. Therefore, ultrahigh purity hydrogen is required for making the fuel cell operation feasible. One of the possible methods for this can be the use of water-gas shift (WGS) reaction.

WGS reaction is an industrially used reaction for enriching the synthetic gas for hydrogen by removal of CO from

Additional Supporting Information may be found in the online version of this article.

Correspondence concerning this article should be addressed to G. Madras at giridhar@chemeng.iisc.ernet.in

the products of a steam reformer.[3] This reaction can be represented as

$$CO + H_2O \Leftrightarrow CO_2 + H_2; \quad \Delta H = -41 \text{ kJ/mol} \qquad (1)$$

The reaction is mainly carried out in the presence of catalysts. Depending on the temperature of operation, the reaction is said to be a low-temperature shift or a high-temperature shift. A typical temperature range is 210–250°C for a low-temperature shift reaction and 310–450°C for the high-temperature shift reaction.[7] The catalysts used for the two temperature ranges are also different. High-temperature shift is used first followed by low-temperature shift conversion. The catalysts used in high-temperature shift are mainly iron oxide catalysts promoted over by chromium oxide working at high CO concentrations. The low-temperature shift catalysts are mainly the ternary solid solutions consisting of $Cu/ZnO/Al_2O_3$.[7–9] These catalysts have been reported to be very efficient for the removal of the final CO impurities from the product.[8]

The reaction is a reversible exothermic reaction and thermodynamically, the formation of the products is favored by low temperatures while pressure has no effect on the equilibrium conversion. Rhodes et al.[7] have given the equilibrium constants for the reaction at different temperatures, which show the expected trend of decrease with temperature. For high-temperature shift, CO conversion and H_2 formation always increase monotonically with temperature, whereas in the case of low-temperature shift, the CO conversion goes through a maximum level. Chen et al.[1] attribute this to the inherent nature of the catalysts and not just the effect of temperature. Thus, the nature of the catalyst indeed has an effect over the conversions that can be achieved apart from the imposed reaction conditions. In view of this, a number of catalysts have been tested for their activity toward the WGS reaction. Atake et al.[3] have shown the use of ternary $Cu/ZnO/Al_2O_3$ catalysts synthesized by homogeneous precipitation technique. The catalysts showed activities higher than the similar catalysts prepared by coprecipitation or impregnation. For application to fuel cells, Galvita and Sundmacher[10] have used iron oxides and other mixed oxides to obtain high-purity hydrogen. Noble metals like Pt, Au, Pd, etc. have been reported to catalyze WGS reaction at low temperatures.[6,8,9,11–20] Apart from this, bimetal substituted compounds have also been tested.[14,18,21] Various supports like CeO_2, ZrO_2, and Al_2O_3 have been used for the catalysts. A number of investigators have made use of mixed supports having ceria-zirconia or ceria-zirconia-alumina.[6,8,15,17,19]

In this study, we have synthesized noble metal ion (Pd and Pt) substituted ceria-based catalysts using solution combustion technique. Using this technique, it is possible to obtain high-ionic dispersion of the noble metals and the crystallites can be limited to nanometer size.[22] We have previously carried out exhaust catalysis (CO oxidation, NOx reduction, three-way catalysis) with similar catalysts[23–26] and established the importance of metal ion substitution and oxidation state of the metal for efficient catalysis. The catalysts showed high rates of conversion of CO at low temperatures. In all the catalysts, the noble metal was substituted in ionic form. Use of such compounds for WGS activity has not been reported and therefore, the activity of these catalysts for the WGS reaction was tested. For testing, reformer outlet conditions were simulated in a laboratory reactor setup. For the design of the reactors and optimizing the process variables, expressions for the parameters influencing the rate of reaction are required. The study provides an insight into the various surface and catalytic processes that take place over the catalyst. The metal-support interactions taking place in the catalyst during the reaction were established. The study provides a rationale for the catalyst design on the basis of the various surface and electronic phenomena taking place during the reaction and the principles can be extended for the synthesis and use of other similar compounds for WGS. Specifically, cheaper metals like Fe or Cr may be examined instead of Pt. A number of empirical rate expressions for concentration and temperature dependence are available in the literature. Here, we have presented the kinetics of the reaction on the basis of catalyst structure. The various possible processes taking place over the catalyst were proposed and tested and the kinetic model equations were derived. As the WGS reaction is a reversible reaction, an exhaustive treatment of the reaction kinetics by considering the competitive adsorption of both reactants and products is proposed.

Experimental

Catalyst synthesis

Noble metal ion substituted ceria was prepared by single-step solution combustion technique. The compounds synthesized were 1% Pd/CeO_2, 2% Pd/CeO_2, 1% Pt/CeO_2, and 2% Pt/CeO_2. All the substitutions were atom percent of the metal ion in ceria. Therefore, all the compounds were essentially solid solutions that can be represented by the formula $Ce_{1-x}M_xO_{2-\delta}$ where M = Pd or Pt and $x = 0.01$ and 0.02 for 1% and 2% substitution, respectively. Cerium ammonium nitrate (Loba Chemie, India) was used as the cerium compound and oxalyldihydrazide (Alfa Aesar, India) was used as the fuel. For Pd substituted compounds, palladium chloride (Merck, India) was used and for Pt substituted compounds, hexachloroplatinic acid (Merck, India) was used.

For the synthesis of $Ce_{1-x}Pd_xO_{2-\delta}$, $PdCl_2$, $(NH_4)_2Ce(NO_3)_6$ and $C_2H_6N_4O_2$ were taken in a molar ratio of x:1−x:2.4 where x represents the substitution. Typically, for the preparation of $Pd_{0.2}Ce_{0.98}O_{2-\delta}$, 10 g of $(NH_4)_2Ce(NO_3)_6$, 0.066 g of $PdCl_2$, and 5.175 g of $C_2H_6N_4O_2$ were taken which was in the molar ratio of 0.02:0.98:2.4, $PdCl_2$:$(NH_4)_2Ce(NO_3)_6$:$C_2H_6N_4O_2$. The aforementioned mixture was taken in a 300 ml borosilicate dish and was added with deionized water to obtain thick slurry. Few drops of nitric acid were added to obtain a clear solution. The dish was then kept in a furnace preheated to 350°C covered with a borosilicate glass plate to avoid the product losses. The solution in the furnace boiled till all the water vaporized. The solution was observed to catch fire instantaneously giving a highly porous and voluminous solid product. The product was then taken out and cooled in desiccators. It was then ground very fine and was heated in the furnace at 500°C for 24 h. $Pd_{0.01}Ce_{0.99}O_{2-\delta}$ and Pt compounds were prepared in an analogous manner taking the precursors in the corresponding molar ratio.

Catalyst characterization

All the catalysts were characterized for their complete structure by powder X-ray diffraction (XRD) and X-ray

photoelectron spectroscopy (XPS). The powder XRD of the samples were carried out on Phillips X'pert diffractometer using CuKα radiations at a scan rate of 0.5°/min and in the 2θ range of 20–85°. XPS was recorded on Thermo Fisher Scientific Multilab 2000 (England) instrument with AlKα radiation (1486.6 eV). The sample was made into a thin pellet (thickness = 0.5 mm) and kept in an ultrahigh vacuum chamber for XPS studies. All the peaks were calibrated with respect to the C1s peak.

WGS catalytic activity tests

The gas phase catalytic studies were conducted using the catalysts prepared earlier in granular form. Highly porous catalyst obtained after synthesis was ground to fine powder. Granules of the size of −50/+100 standard ASTM mesh were made. The catalysts were then placed in a 4 mm ID quartz tube packed at both the sides by quartz wool. The reactor was heated from outside using an electric heater equipped with a PID temperature controller and K-type chromel-alumel thermocouple. The reactant gases, CO (10.33% in N_2) (Chemix Speciality Gases, Bangalore, India), N_2, H_2, and CO_2 (all from Vinayaka Gases Pvt. Ltd., Bangalore, India) were supplied from the cylinders through high precision fine control needle valves. The flow rates of the gases were measured using a flow meter. The gases were mixed in a mixing chamber and were then sent to the reactor. Water was fed with the help of a high-pressure HPLC pump (AA-100-S-2-CC, Eldex Laboratories, USA). The entire line was heated and maintained at temperature at 150°C to ensure that water is vaporized and reaches the reactor as a homogeneous mixture.

Before the reaction, the catalysts were heated in the stream of N_2 at 150°C for 1–2 h to remove all the moisture and entrapped/adsorbed gases. For carrying out the kinetic study, the reactor was operated in differential mode by taking a small amount of catalyst such that the total conversion did not exceed 10–15%. The rates were calculated by tracing the conversion obtained at different temperatures. All the reactions were isothermal reactions. Other reactions showing higher conversions were carried with higher amounts of catalyst. The unreacted water was condensed by passing the gas through a condenser placed in an ice bath. The dry products were analyzed by an online gas chromatograph (Nano HP-I, Mayura Analyticals Pvt., Ltd., Bangalore, India) equipped with an autosampler and a combination of columns (Hayesep-A and two molecular sieve columns) for a single step separation of CO, CO_2, and H_2 (also methane and other hydrocarbons that were not observed). CO and CO_2 were analyzed by a flame ionization detector, whereas H_2 was detected by a thermal conductivity detector.

Results and Discussion

Structural studies

Both CeO_2 and substituted CeO_2 crystallized in fluorite structure. This can be seen from XRD patterns, which is shown in Supporting Information Figure S1. No metal peaks were observed for the substituted compounds. Even the magnified *y*-axis (not shown) did not show any metal or metal oxide peak. Therefore, it can be inferred that the noble metals occupied the lattice positions of cerium. The diffraction lines of substituted compounds showed broadening when compared with those of pure ceria showing a decrease in the crystallite size. The detailed structural analysis and Rietveld refined pattern have been previously reported.[24–29] All the crystallite sizes were between 8 and 12 nm (confirmed by TEM). Thus, the compounds were nanocrystalline solids. In our previous studies, we could detect even highly dispersed impregnated metal peak from XRD.[29] In the currently synthesized catalysts, absence of metal peak indicates complete substitution of metal in ionic form. TEM images before and after the reaction were also recorded showing a small increase in crystallite size after reaction, but diffraction lines corresponding to metal were negligible confirming that the metal is dispersed in ionic form.[27,28]

The XPS of all the elements present in the catalyst were recorded. All the peaks were calibrated with respected to the C1s peak observed at a binding energy of 284.5 eV. It can be seen from the 3d core level spectra of Pd, given in Supporting Information Figures S2a,b, that the peaks were observed at 337.5 and 342.9 eV, corresponding to $3d_{5/2–3/2}$ spin-orbit doublets for both the Pd substituted compounds. Pd metal binding energies were observed to be 335 and 340.5 eV in our previous studies.[25] Clearly, Pd was substituted in +2 state. 4f core level spectra for Pt are given in Supporting Information Figures S3a,b. The spectra were very wide and hence mixed valance states were present. The spectra were decomposed to obtain three sets of spin-orbit doublets corresponding to the +4, +2, and zero states (see Supporting Information Figure S3). From the decomposed spectra, all the three oxidation states can be observed to be present. The relative amounts of the three oxidation states were calculated. For 1% Pt/CeO_2, the relative contribution of the 0, +2, and +4 states was 30%, 40%, and 30%, whereas for 2% Pt/CeO_2, it was 35%, 40%, and 25%, respectively. The XPS of the catalysts were recorded before and after the reaction to observe the changes in the oxidation state of the noble metals. No significant changes in metal content, present in small quantity, were observed and the ionic state continued to be prevalent. Our previous work on the deactivation of the catalysts over long-time exposure to the WGS conditions has shown the metals to be in ionic state after nearly 22 h of cyclic operation.[30] No significant changes in the XPS of the noble metal were observed before and after the reaction. In this study also, the ionic dispersion continued after the reaction. XPS of Ce3d is given in Supporting Information Figure S4. Ce was present mainly in +4 state.

Catalytic reactions

Two percent CO balanced with N_2 to make a total flow of 100 ml/min was passed over 100 mg of catalyst. The flow of water was 0.1 ml/min (liquid) and space velocity of 95,000/h was maintained. Figures 1 and 2 show the CO conversion and H_2 generation profiles with temperature, respectively. The ordinate for CO has been scaled with the inlet CO concentration in the feed, whereas for H_2 generation, it is scaled with the amount of H_2 that would have been formed if whole of the CO were converted to CO_2. With Pt substituted catalysts, 90–95% conversions were obtained at 275°C. The activity did not increase much with an increase in substitution from 1 to 2%. With Pd substituted compounds, the temperature

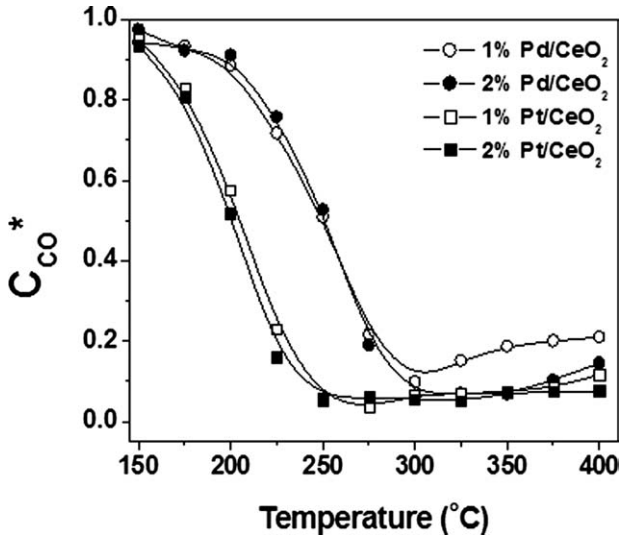

Figure 1. Variation of the normalized concentration profiles of CO with temperature.

requirements were higher. The initial activity was lesser in this case, but the final conversions obtained were nearly the same for all the catalysts. It was found that for all the catalysts, the temperature range of 250–275°C was the optimum for CO consumption and H_2 generation. After this, CO conversion was found to decrease. The H_2 generation profile shows that there was a corresponding increase in the H_2 till 250°C after which no further increase was observed. At temperatures as high as 400°C, a decrease in H_2 concentration was observed due to the reversibility of the reaction.

Experiments were carried out with a mixture of gases and different amounts of catalysts. The reactant mixture had a dry gas composition of 2% CO, 10% CO_2, 40% H_2, and balance N_2. The dry gas flow was maintained at 100 ml/min at STP. The CO conversion profiles are shown in Figure 3. The reaction is an exothermic equilibrium reaction and therefore, the equilibrium conversion decreases with temperature. The dotted line shows the equilibrium conversion. Two percent Pt substituted compound showed the highest activity with the conversions reaching near equilibrium at 250°C with 500 mg of the catalyst. The highest conversion obtained was nearly 88% with this catalyst. The effect of the species present in the reaction mixture can be seen easily by comparing Figures 1 and 3. With Pd substituted compounds, only 40% conversion was possible. CO was observed to have a decrease in conversion at temperatures above 250°C in all the cases. The CO conversion profiles were sigmoidal for all the catalysts showing a light off at nearly 200–225°C. After the light off, the rate of conversion decreased (Figure 3). This was especially observed in reactions with high amounts of catalyst. Radhakrishnan et al.[6] have observed high rates and equilibrium conversions with similar reactant mixture and ceria-zirconia mixed oxides at nearly 300°C with Pt metal, which showed higher activity than Pd. Although the metals were used in impregnated form, the migration of the metal to ionic form is possible during the thermal treatment step and high temperatures of reaction.[31] Boaro et al.[19] have also observed equilibrium conversions in similar temperature range with Pt doped mixed oxides. Fu et al.[9] found the activation energy to be independent of percentage of Pt in the catalyst in the La/CeO_2 system and a decrease in activation energy was found with increasing noble metal substitution. Bakhmutsky et al.[32] observed equilibrium conversions over Pd/CeO_2, $Pd/Ce_{0.5}Pr_{0.5}O_{2-x}$ and Pd/Pr_6O_{11} catalysts synthesized by thermal decomposition method. High surface area catalysts were synthesized with high dispersion of Pd. It was found that the reducibility of the catalyst should be optimum for high activity. There have been investigations on the effect of redox properties of the support on the activity toward WGS and other redox reactions.[33,34] Similarly, Baldychev et al.[35] observed high rates of WGS with Fe supported over alumina and zirconia. The rates were found to be dependent on the changes in the oxidation states of Fe during the redox cycle. With high dispersion, just 1% Pd was found to be sufficient for achieving high rates and conversion. In our catalysts, substituting of metal in ionic form resulted in a high dispersion of the active metal and the equilibrium conversions at relatively lesser temperatures were observed.

Heterogeneous catalysis involves the reaction taking place over the surface of the catalyst via a number of steps involving adsorption of the reactants, surface reaction, desorption of products, and the various transport processes. To derive a qualitative expression describing the kinetics of the reaction, the rate limiting step must be known. For this, the reactions were carried out with 100 mg of the different catalysts at 225°C taking different initial concentration of CO in the feed balanced with N_2 and the amount of H_2 produced was traced. This is shown in Figure 4. It can be noted that the increase in feed CO concentration did not result in a linear increase in the production of H_2. Hence, the initial rate of reaction did not follow a linear relation with the initial reactant concentration but shows saturation. This is a characteristic of reactions controlled by the surface reaction kinetics.[36] Therefore, it can be concluded that the limiting step in the mechanism is the surface reaction and not the adsorption or desorption of the species. This was made use of while deriving the model equations.

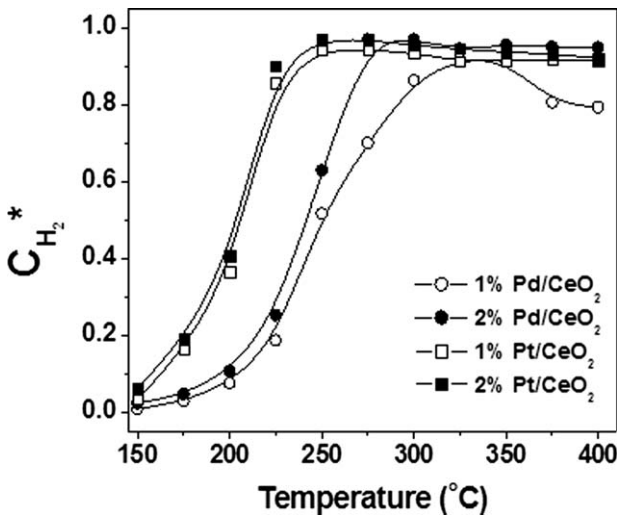

Figure 2. Variation of the normalized concentration profiles of H_2 with temperature.

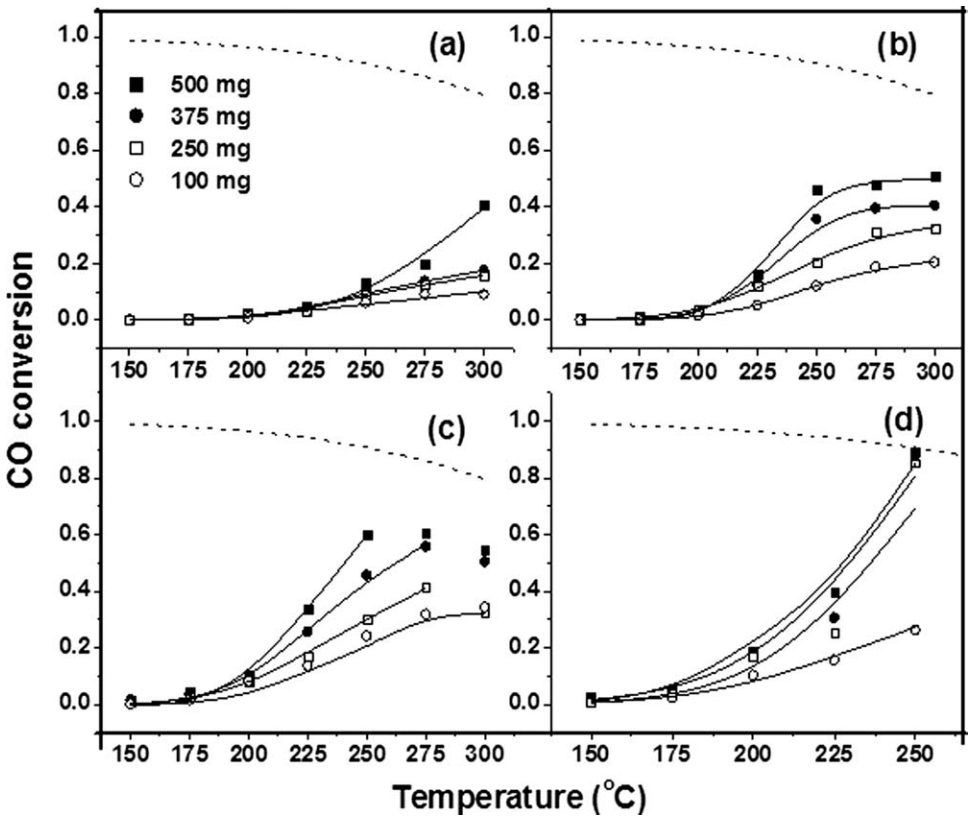

Figure 3. Variation of CO conversion with temperature for the different catalysts.

(a) $Ce_{0.99}Pd_{0.01}O_{2-\delta}$, (b) $Ce_{0.98}Pd_{0.02}O_{2-\delta}$, (c) $Ce_{0.99}Pt_{0.01}O_{2-\delta}$, and (d) $Ce_{0.98}Pt_{0.02}O_{2-\delta}$. Symbols represent the experimental values, lines represent the model correlations of mechanism C.

Figure 5 shows Arrhenius plot in which the natural log of initial rate is plotted against the inverse of the absolute temperature. All the plots showed significant deviation from linearity. From the conversion plots (Figure 3), it can be observed that there occurred a light off and at higher temperatures the conversions were not affected much by temperature. This shows the presence of mass transfer effects. Similar observations have been reported by Haye et al.[37] for three-way catalysts where mass transfer limitations were prominent after the light off. For heterogeneous catalysis, transport processes are important and have weak temperature

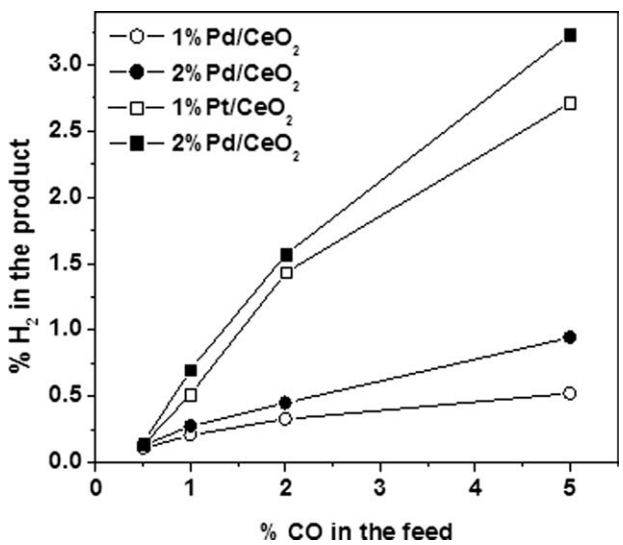

Figure 4. Variation of the H_2 concentration with different inlet CO concentrations.

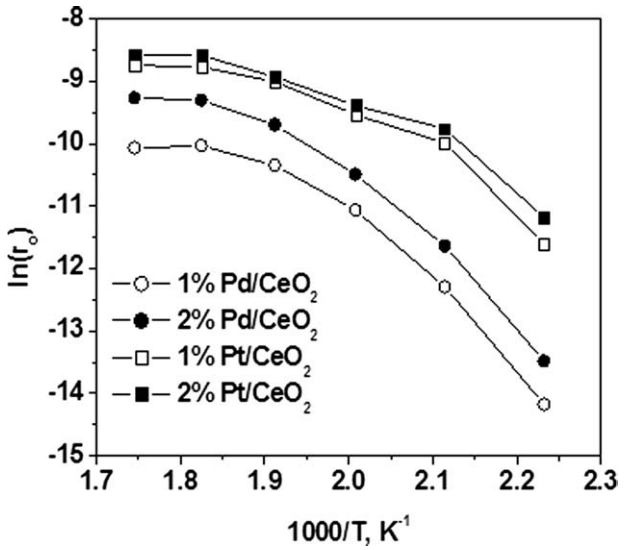

Figure 5. Arrhenius plot showing the variation of initial rate with temperature.

dependence when compared with the exponential dependence of rate given by Arrhenius law. For reaction over a large temperature range, different regimes of rate controlling processes are observed each signified by a change in temperature dependence given by the slope of Arrhenius plot. The highest slopes are obtained at lower temperatures when the reaction is controlled by the kinetics. With the increase in temperature, the temperature dependence decreases and at very high temperatures, the reaction rate become almost independent of the temperature with activation energy of 3–5 kJ/mol.[38] In this region, the rate is external diffusion controlled and for intermediate temperatures, the rate is internal diffusion controlled. Figure 5 shows similar trends. The reaction rates were not influenced significantly above 225°C. Moreover, at this temperature, the reaction did not reach equilibrium conversion. Therefore, the rate of reaction was limited because of the effect of mass transfer and not equilibrium.

Model for the reaction kinetics

WGS has been studied extensively as it is one of the reactions involved in Fischer–Tropsch's process[39] and steam reforming of hydrocarbons.[40] Models describing the kinetics using Langmuir–Hinshelwood mechanism has been reported assuming the adsorption of CO over the active metal.[40–42] This approach was used earlier mainly to describe the kinetics over the conventional catalysts. Another approach adopted was finding the power law type kinetics by tracing the effect of each of the chemical species.[15,42–46] Some investigators have used the redox chain mechanism for describing the kinetics.[47,48] Grenoble and Estadt gave a detailed description of WGS reaction over a number of noble and base metal supported alumina on the basis of intermediate formic acid formation.[40] The main argument behind this was the two possible ways in which formic acid could dissociate. In the first pathway, CO and H_2O may be formed whereas in the other, CO_2 and H_2 may be formed. Since WGS requires both of these sets, intermediate formic acid formation was proposed. In our case, we have used substituted ceria as catalysts. Ceria is a reducible oxide and the noble metals are substituted in ionic form. Therefore, redox processes are expected to be taking place over the catalyst. We propose the possible elementary steps taking place over the surface of the catalyst and check their consistency for the experimental data. On the basis of the values of the pre-exponential factor or the activation energy, we accept or discard the mechanism. We tested the following mechanisms for WGS activity over the catalysts.

Mechanism A (Eley–Rideal mechanism)

$$CO + S_M \Leftrightarrow CO_M \tag{2.1}$$

$$CO_M + H_2O \rightarrow CO_2 + H_2 + S_M \tag{2.2}$$

Mechanism B (Langmuir–Hinshelwood mechanism)

$$CO + S_M \Leftrightarrow CO_M \tag{3.1}$$

$$H_2O + S_M \Leftrightarrow H_2O_M \tag{3.2}$$

$$CO_M + H_2O_M \rightarrow CO_2 + H_2 + 2S_M \tag{3.3}$$

Mechanism C

$$CO + S_M \Leftrightarrow CO_M \tag{4.1}$$

$$H_2O + 'v' \rightarrow 'o' + H_2 \tag{4.2}$$

$$CO_M + 'o' \rightarrow CO_2 + 'v' + S_M \tag{4.3}$$

$$H_2 + S_M \Leftrightarrow H_{2_M} \tag{4.4}$$

$$CO_2 + 'v' \rightarrow 'o' + CO \tag{4.5}$$

$$H_{2_M} + 'o' \rightarrow H_2O + 'v' + S_M \tag{4.6}$$

In the aforementioned equations, the subscript "M" represents the adsorption site of the metal over the catalyst. Thus CO_M represents CO molecules adsorbed over metal ion. 'v' represents the oxide ion vacancy and 'o' the intermediate species formed over the oxide ion vacancy. Eley–Rideal mechanism assumes the adsorption of CO molecule over the metal ions and reaction of H_2O directly with the adsorbed CO. This is represented by mechanism A. CO gets adsorbed over the metal ion represented by M, which may be Pd or Pt. H_2O in the stream reacts with the adsorbed CO and the products get desorbed thereby making the adsorption site free and completing the catalytic cycle.

The Langmuir–Hinshelwood mechanism given as mechanism B assumes the adsorption of both the species. Adsorption over metal ion is considered. Oxide ion vacancies can also act as adsorption sites. Nevertheless, as no significant conversion was observed over unsubstituted ceria, it is fair to assume that only metal ions were the sites for adsorption and the probability of adsorption of CO over oxide ion vacancies was negligible.

Both of the aforementioned reaction mechanisms, A and B, are based on the single site utilization, i.e., adsorption and surface reactions over the metal ion present in the catalyst. However, in the case of ceria compounds, the oxides are rarely stoichiometric.[49] For low-temperature shifts, Boaro et al.[19] in their experiments on WGS over ceria-zirconia mixed catalysts, have found the catalytic activity to be dependent on the nature of the support. Therefore, it is important to take into consideration the processes taking place over the support. Reduced ceria has oxide ion vacancies. Further, the substitution of metals in ionic form results in the formation of more anionic vacancies to compensate for the charge balance. These oxide ion vacancies are expected to play a vital role in the redox catalytic processes. The vacancies are electron deficient sites and, therefore, can provide an oxidizing environment. In this manner, the reduced oxide along with the metal ions act as a host for redox processes and particularly in the case of WGS reaction, the vacancies aid in activating water.[50]

Therefore, we have proposed mechanism C based on the utilization of dual sites, i.e., metal ions and oxide ion vacancies simultaneously. There have been reports of different site utilization for CO and H_2O adsorption. In iron oxide based catalysts, the mechanism assuming CO adsorption over metal and H_2O dissociation over the oxide giving ferrous-ferric ion cycle has been reported.[47] Kubsh et al.[52] have used the adsorption-regeneration path for WGS over magnetite

assuming water splitting to H_2 and giving intermediate oxygen species. Recently, Azzam et al.[53,54] have shown the effect of support for the adsorption of various species for WGS over noble metal impregnated ceria, titania and zirconia and considered the dissociation of water over the support. For CO oxidation and NOx reduction, we have found the dual site utilization to be the most suitable mechanism describing the kinetics of the reaction.[24–26] Therefore, we investigate this mechanism for WGS.

In mechanism C, CO is assumed to be adsorbed over the metal ion and water dissociatively over the oxide ion vacancy. The surface reaction between the two adsorbed species results in the formation of products which on desorption restores the catalyst. This is given in steps 4.1–4.3.

WGS is a reversible reaction. Therefore, the rates of reaction are dependent on the products present in the feed gas. The influence of H_2 and CO_2 on conversions can be seen clearly from the large differences in the conversions shown in Figures 1 and 3. Therefore, we further extend the mechanism to account for the overall equilibrium of the reaction. Steps 4.4 and 4.5 represent the competitive adsorption of the reactants and products. With the analogy of dissociation of oxidizing H_2O over vacancies and adsorption of CO over metal, we propose the competitive dissociation and adsorption of CO_2 and H_2 over vacancy and metal ion, respectively. The metal ions in the catalyst were present in the oxidized state. Therefore, any species having a tendency toward oxidation of the metals were not very likely to get adsorbed over the metals. Therefore, CO provides a reducing environment for the metal and itself gets oxidized to CO_2. Similarly, we can expect the adsorption of H_2 over the metal ion rather than that of CO_2. The net composition of the product depends on the relative magnitude of the two competitive processes that are dependent on the concentration and temperature, which are the natural variables describing the equilibrium of a reaction. A major fraction of the feed consists of N_2, which is inert. It may cause hindrance in the reaction by adsorption. However, following the previous arguments, N_2 is susceptible to neither oxidation nor reduction. Therefore, it is fair to assume no adsorption of N_2 during the reaction.

The rate expressions for the various mechanisms were derived. The final expressions obtained were given as follows:

Mechanism A

$$r = \frac{K_1 k_2 [\mathrm{CO}][\mathrm{H_2O}]}{1 + K_1[\mathrm{CO}]} \tag{5}$$

Mechanism B

$$r = \frac{K_1 K_2 k_3 [\mathrm{CO}][\mathrm{H_2O}]}{(1 + K_1[\mathrm{CO}] + K_2[\mathrm{H_2O}])^2} \tag{6}$$

Mechanism C

$$r = \frac{\{K_1 k_3 [\mathrm{CO}](1 + K_4[\mathrm{H_2}]) - K_4 k_6 [\mathrm{H_2}](1 + K_1[\mathrm{CO}])\}(k_2[\mathrm{H_2O}] + k_5[\mathrm{CO_2}])}{(1 + K_1[\mathrm{CO}])(1 + K_4[\mathrm{H_2}])(k_2[\mathrm{H_2O}] + k_5[\mathrm{CO_2}]) + (1 + K_4[\mathrm{H_2}])K_1 k_3[\mathrm{CO}] + (1 + K_1[\mathrm{CO}])K_4 k_6[\mathrm{H_2}]} \tag{7}$$

The details of the derivation and the underlying assumptions can be found in Appendix A of the Supporting Information. K_i in the equations represents the equilibrium constant for the ith step and k_i represents the corresponding rate constant. The quantities within [] represent the molar concentration. Both K_i and k_i are temperature dependent. We model the rate constants using the Arrhenius law, so that the following equation holds

$$k_i = A_i \exp(-E_i/RT) \tag{8}$$

$$k_i = A_i \exp(B_i/T) \tag{9}$$

where A_i and E_i represent frequency factor and activation energy of ith step respectively and B_i is the parameter used for optimization, $B_i = -E_i/R$. Following Granger et al.,[55] the equilibrium adsorption can be modeled as Arrhenius type relation

$$K_i = A_i \exp(-\Delta H_{\mathrm{ads},i}/RT) \tag{10}$$

$$K_i = A_i \exp(B_i/T) \tag{11}$$

where $\Delta H_{\mathrm{ads,i}}$ is the heat of adsorption of the reactants.

The conversions were predicted on the basis of the aforementioned rate expressions for reactions over all the catalysts. It can be seen from Figure 3 that use of 100 mg of the catalyst resulted in very low conversions. In this limit, the catalyst bed can be assumed to be nearly gradientless and the bed can be approximated to be a perfectly mixed system described by the equations of a CSTR given as

$$x = Wr/F \tag{12}$$

where x is the conversion, r is the rate of reaction per unit catalyst weight per unit time, W is the weight of catalyst taken and F is the molar flow rate of the species whose conversion is followed. Using the known values of W and F and derived rate expressions, an expression for the conversion as a function of temperature and concentration was derived. The expressions for the equilibrium adsorption of CO and H_2 over the metal ions were taken from the literature. The expressions are available for the adsorption of gases over the metal in zero state. However, a study by Bera et al.[27] showed that the equilibrium adsorption of CO over Pt metal in different oxidation states is the same with a value of sticking coefficient of 0.12. It was found experimentally that the adsorption of CO over Pt/CeO_2 system was the same over both Pt metal as well as the ionic Pt. The study also compared adsorption over Pt/Al_2O_3 system and a 10-fold decrease in adsorption was observed. This clearly showed the involvement of the support for the surface processes. Higher dispersion of ions in CeO_2 is possible thereby making it a better support material for the reactions involving CO. Therefore, the expression for the equilibrium adsorption over the metals was used directly as an estimate of the adsorption over metal ions. A sensitivity analysis was carried out for the different parameters involved in the model affecting the rate of reaction. The parameters

Table 1. Optimized Rate Expressions for the Various Reaction Mechanisms

Mechanism	Parameter	Expression*			
		$Ce_{0.99}Pd_{0.01}O_{2-\delta}$	$Ce_{0.98}Pd_{0.02}O_{2-\delta}$	$Ce_{0.99}Pt_{0.01}O_{2-\delta}$	$Ce_{0.98}Pd_{0.02}O_{2-\delta}$
A	K_1	$10^{15.5}\exp(14950/T)^{\dagger}$	$10^{15.5}\exp(14950/T)^{\dagger}$	$4.3\times10^{14}\exp(16165/T)^{\ddagger}$	$4.3\times10^{14}\exp(16165/T)^{\ddagger}$
	k_2	$(243\pm16)\exp\{(-5173\pm103)/T\}$	$(382\pm12)\exp\{(-5050\pm64)/T\}$	$(107\pm35)\exp\{(-4920\pm564)/T\}$	$(101\pm12)\exp\{(-4802.76\pm899)/T\}$
B	K_1	$10^{15.5}\exp(14950/T)^{\dagger}$	$10^{15.5}\exp(14950/T)^{\dagger}$	$4.3\times10^{4}\exp(16165/T)^{\ddagger}$	$4.3\times10^{4}\exp(16165/T)^{\ddagger}$
	K_2	$10^{13}\exp(5087/T)^{\S}$	$10^{13}\exp(5087/T)^{\S}$	$10^{13}\exp(5087/T)^{\S}$	$10^{13}\exp(5087/T)^{\S}$
	k_3	$(10^{4}\pm545)\exp\{(4505\pm154)/T\}$	$(1.72\times10^{4}\pm3425)\exp\{(4865\pm79)/T\}$	$(2310\pm686)\exp\{(6516\pm214)/T\}$	$(1.52\times10^{4}\pm7998)\exp\{(5247\pm769)/T\}$
C	K_1	$10^{15.5}\exp(14950/T)^{\dagger}$	$10^{15.5}\exp(14950/T)^{\dagger}$	$4.3\times10^{14}\exp(16165/T)^{\ddagger}$	$4.3\times10^{14}\exp(16165/T)^{\ddagger}$
	k_2	$1.7\times10^{13}\exp(-12030/T)$	$1.3\times10^{10}\exp(-7195/T)$	$3.2\times10^{6}\exp(-6089/T)$	$2.3\times10^{7}\exp(-7157/T)$
	k_3	$(1.5\times10^{5}\pm1354)\exp\{(-3996\pm65)\}/T\}$	$(6.2\times10^{7}\pm4657)\exp\{(-3645\pm726)\}/T\}$	$(303\pm53)\exp\{(-3421\pm169)\}/T\}$	$(280\pm32)\exp\{(-3150\pm98)\}/T\}$

*Activation energy, kJ/mol; frequency factor, mol/(g s).
†Taken from Ref. [56].
‡Taken from Ref. [57].
§Taken from Ref. [58].

were determined by nonlinear regression using the software Origin 7.5. The rate parameters were obtained for the proposed mechanisms. It was found that the rate of reaction was a weak function of the adsorption step. After establishing the parameters, the adsorption expression was also treated as a variable and within 95% confidence, no significant differences were found between the two results. The optimized rate parameters for Pd and Pt substituted catalysts are given in Table 1.

The Eley–Rideal mechanism predicts higher activation energies. Moreover, this mechanism assumes only CO adsorption over the metal. This makes the reaction kinetics independent of the support, i.e., the mechanism predicts same catalyst activity over ceria, zirconia, alumina, and even the mixed oxides as long as the adsorbent metal remains the same. This is clearly not the case and different activities have been found by various investigators for different supports.[19,50–54] From the analysis of the rate parameters, it can be concluded that the reaction did not follow Langmuir–Hinshelwood mechanism. For all the four catalysts, the activation energies were negative. Therefore, we discard mechanisms A and B on the basis of the unrealistic values of the rate parameters.

It can be seen that mechanism C best describes the kinetics. The apparent activation energies for 1% Pd/CeO_2, 2% Pd/CeO_2, 1% Pt/CeO_2, and 2% Pt/CeO_2 are 33 kJ/mol, 30 kJ/mol, 28 kJ/mol, and 26 kJ/mol, respectively. These values were lower when compared with the other ceria-based catalysts reported for the WGS reaction. A detailed comparison of rates and activation energies from the various studies[9,30,32,35,59–62] are given in Supporting Information Table S1. It is also interesting to note that the model has correctly predicted the relative rates of the various elementary steps proposed. From Figure 4, it was concluded that the surface reaction was the rate limiting step. It can be indeed shown from the relative values of the rate constants of steps 2 and 3 of mechanism C that dissociative chemisorption of water over the oxide ion vacancies was much faster than the surface reaction. The lines in Figure 3 show the model predictions following mechanism C. The optimization was carried taking the experimental conversions from 100 mg of the catalyst. Only parameters of Eqs. 4.1–4.3 were optimized keeping the rate coefficients for Eqs. 4.4–4.6 as zero. This described the forward reaction. From the curves, it can be seen that the model predicts the conversions fairly well. However, at higher conversions and temperatures, considerable deviation was observed. This may be due to plug-flow conditions at very high conversion as well as due to mass transfer limitations at very high temperatures. Moreover, in all the four cases, the model predicted lower conversion at high temperatures, especially with high catalyst weight. It is consistent with the fact that the conversion obtained in with plug flow conditions are higher than that obtained with CSTR conditions. The predicted conversions were low because the model assumes CSTR conditions.

The complete mechanism is able to account for the reverse reaction and possible adsorption of all the species involved in the reaction. However, in the temperature range in which this study was carried out, only forward reaction takes place. Moreover, for syn-gas purification, and hydrogen production, the main interest is to describe the forward reaction. Therefore, it is fair to assume negligible influence of

the reverse reaction rate parameters on the reaction rate. Zhdanov[63] has studied the adsorption of H_2 over Pt and proposed,

$$K = 10^{13} \exp(9895/T) \tag{13}$$

From the aforementioned equation and the ones given in Table 1, we find that the heat of adsorption of CO over the metal is much higher when compared with that of H_2 and hence, at low enough temperatures, adsorption of CO will be much higher than H_2. The rate of step 4.1 is four orders of magnitude higher than that of step 4.4. Therefore, steps 4.1–4.3 proposed in mechanism C prominently take place. The adsorption of H_2 is weak and the corresponding reverse reaction does not take place at least up to 300°C. Moreover, WGS is an exothermic reaction and has a negative value of Gibbs' free energy. Therefore, in the temperature range studied here, the limiting case of this mechanism describes the kinetics fairly well. However, it should be noted here that due to the presence of mass transfer limitations at high temperatures (>250°C), the kinetics developed in this study is expected to hold only at temperatures below 225°C. With more data, larger temperature range, and high-space velocities, it may possible to obtain the optimized parameters for the complete mechanism and the kinetics of both forward and reverse reaction can be described by this mechanism.

Conclusions

WGS activity was tested over Pt and Pd substituted nanocrystalline CeO_2 catalysts. The catalysts showed good activity toward the reaction that yielded equilibrium conversions around 250°C. For the reaction with only CO, an increase in metal ion substitution did not show any considerable increase in activity, whereas for the reactions in the presence of H_2 and CO_2, reactivity increased by increasing the substitution. Pt substitution was found to be better when compared with Pd substitution. However, Pd also showed good catalytic activity at relatively higher temperatures. The mechanism involving the adsorption of CO over the metal ion and dissociation of water over the oxide ion vacancies was found to describe the kinetics of the reaction. The reaction was surface reaction controlled and the effect of temperature on the equilibrium conversion was observed with the highest conversion being limited by the equilibrium of the reaction.

Acknowledgments

G.M. gratefully acknowledges the Department of Science and Technology, India, for the Swarnajayanti Fellowship. M.S.H. gratefully acknowledges the Indian Council for Agricultural Research (ICAR), Government of India, for funding.

Literature Cited

1. Chen WH, Lin MR, Jiang TL, Chen MH. Modeling and simulation of hydrogen generation from high-temperature and low-temperature water gas shift reactions. *Int J Hydrogen Energy*. 2008;33:6644–6656.
2. Hellman HL, van den Hoed L. Characterising fuel cell technology: challenges of the commercialisation process. *Int J Hydrogen Energy*. 2007;32:305–325.
3. Atake I, Nishida K, Li D, Shishido T, Oumi Y, Sano T, Takehira K. Catalytic behaviour of ternary $Cu/ZnO/Al_2O_3$ systems prepared by homogeneous precipitation in water-gas shift reaction. *J Mol Catal A: Chem*. 2007;275:130–138.
4. Schmidt VM, Brocheerhoff P, Hohlein B, Menzer R, Stimming U. Utilization of methanol for polymer electrolyte fuel cells in mobile systems. *J Power Sources*. 1994;49:299–313.
5. Vidal F, Busson B, Six C, Pluchery O, Tadjeddine A. SFG study of methanol dissociative adsorption at Pt (100), Pt(110) and Pt(111) electrodes surfaces. *Surf Sci*. 2002;485:502–503.
6. Radhakrishnan R, Willigan RR, Dardas Z, Vanderspurt TH. Water gas shift activity of noble metals supported on ceria-zirconia oxides. *AIChE J*. 2006;52:1888–1894.
7. Rhodes C, Hutchings GJ, Ward AM. Water-gas shift reaction: finding the mechanistic boundary. *Catal Today*. 1995;23:43–58.
8. Fonseca AA, Fisher JM, Ozkaya D, Shannon MD, Thompsett D. Ceria-Zirconia supported Au as highly active low temperature water-gas shift catalyst. *Top Catal*. 2007;44:223–235.
9. Fu Q, Saltsberg H, Flytzani-Stephanopoulos M. Active non-metallic Au and Pt species on ceria-based water-gas shift catalyst. *Science*. 2003;301:935–938.
10. Galvita V, Sundmacher K. Cyclic water gas shift reactor (CWGS) for carbon monoxide removal from hydrogen feed gas for PEM fuel cells. *Chem Eng J*. 2007;134:168–144.
11. Si R, Flytzani-Stephanopoulos M. Shape and crystal-plane effects of nanoscale ceria on the activity of Au-CeO_2 catalysts for the water-gas shift reaction. *Angew Chem Int Ed*. 2007;47:2884–2887.
12. Rodrigues JA, Ma S, Liu P, Hrbek J, Evens J, Perez M. Activity of CeO_2 and TiO_2 nanoparticles grown on Au(111) in the water-gas shift reaction. *Science*. 2007;318:1757–1760.
13. Khan MMT, Halligudi SB, Shukla S. Oxidative addition of water to Ru(II) catalyst K[Ru(II)(Hedta)(CO)]: homogeneous catalysis of the water-gas shift reaction under ambient conditions. *Angew Chem Int Ed Engl*. 1988;27:1735–1736.
14. Kambe N, Morimoto F, Kondo K, Sonoda N. Water gas shift reaction with aid of selenium/platinum catalyst. *Angew Chem Int Ed Engl*. 1980;19:1007.
15. Germani G, Schuurman Y. Water-gas shift kinetics over μ-structured $Pt/CeO_2/Al_2O_3$ cataysts. *AIChE J*. 2006;52:1806–1813.
16. Danh NH, de Farias AMD, Fraga MA. Characterization and activity of vanadia-promoted Pt/ZrO_2 catalysts for the water-gas shift reaction. *Catal Today*. 2008;138:235–238.
17. Panagiotopoulou P, Papavasiliou J, Avogouropolous G, Ioannides T, Kondarides DI. Water-gas shift activity of doped Pt/CeO_2 catalysts. *Chem Eng J*. 2007;134:16–22.
18. Sekine Y, Takamatsu H, Aramaki S, Ichishima K, Takada M, Matsukata M, Kikuchi E. Synergistic effect of Pt or Pd and perovskite oxide for water gas shift reaction. *Appl Catal A: Gen*. 2009;352:214–222.
19. Boaro M, Vicario M, Llorca J, de Leitenburg C, Dolcetti G, Trovarelli A. A comparative study of water gas shift reaction over gold and platinum on supported ZrO_2 and CeO_2-ZrO_2. *Appl Catal B: Environ*. 2004;52:225–237.
20. Kim WB, Voitl T, Rodrigues-Rivera J, Dumesic JA. Powering fuel cells with CO via aqueous polyoxomethylates and gold catalysts. *Science*. 2004;305:1280–1283.
21. Fox EB, Velu S, Engelhard MH, Chin YH, Miller JT, Kropf J, Song C. Characterization of CeO_2-supported Cu-Pd bimetallic catalyst for the oxygen-assisted water-gas shift reaction. *J Catal*. 2008;260:358–370.
22. Hegde MS, Madras G, Patil KC. Nobel metal ionic catalysts. *Acc Chem Res*. 2009;42:704–712.
23. Gayen A, Baidya T, Biswas K, Roy S, Hegde MS. Synthesis, structure and three way catalytic activity of $Ce_{1-x}Pt_{x/2}Rh_{x/2}O_{2-\delta}$ (x=0.01-0.02) nano-crystallites: synergistic effect in bimetal ionic catalysts. *Appl Catal A: Gen*. 2006;315:135–146.
24. Roy S, Marimuthu A, Hegde MS, Madras G. High rates of NO and N_2O reduction by CO, CO and hydrocarbon oxidation by O_2 over nano-crystalline $Ce_{0.98}Pd_{0.02}O_{2-\delta}$: catalytic and kinetic studies. *Appl Catal B: Envron*. 2007;71:23–31.
25. Roy S, Marimuthu A, Hegde MS, Madras G. NO reduction by H_2 over nano-$Ce_{0.98}Pd_{0.02}O_{2-\delta}$. *Catal Commun*. 2008;9:101–105.
26. Roy S, Marimuthu A, Hegde MS, Madras G. Pd ion substituted CeO_2: a superior de-NOx catalyst to Pt or Rh doped ceria. *Catal Commun*. 2008;9:811–815.

27. Bera P, Patil KC, Jayaram V, Subbanna GN, Hegde MS. Ionic dispersion of Pt and Pd ions by combustion method: effect of metal-ceria interaction on catalytic activities for NO reduction and CO and hydrocarbon oxidation. *J Catal*. 2000;196:293–301.
28. Bera P, Malwadkar S, Gayen A, Satyanarayana CVV, Rao BS, Hegde MS. Low temperature water-gas shift reaction on combustion synthesized $Ce_{1-x}Pt_xO_2$ catalyst. *Catal Lett*. 2004;96:213–219.
29. Baidya T, Marimuthu A, Hegde MS, Ravishankar N, Madras G. Higher catalytic activity of nano-$Ce_{1-x-y}Ti_xPd_yO_2$ compared to nano-$Ce_{1-x}Pd_xO_2$ for CO oxidation and N_2O and NO reduction by CO: role of oxide ion vacancy. *J Phys Chem C*. 2007;111:830–839.
30. Sharma S, Deshpande PA, Hegde MS, Madras G. Nondeactivating nanosized ionic catalysts for water-gas shift reaction. *Ind Eng Chem Res*. 2009;48:6535–6543.
31. Pierre D, Dang W, Flytzani-Stephanopoulos M. The importance of strongly bound Pt-CeO_x species for the water-gas shift reaction: catalyst activity and stability evolution. *Topic Catal*. 2007;46:363–373.
32. Bakhmutsky K, Zhou G, Timothy S, Gorte RJ. The water-gas shift reaction on Pd/ceria-praseodymia: the effect of redox thermodynamics. *Catal Lett*. 2009;129:61–65.
33. Zhou G, Shah PR, Gorte RJ. A study of cerium-manganese mixed oxides for oxidation catalysis. *Catal Lett*. 2008;120:191–197.
34. Zhou G, Hanson J, Gorte RJ. A thermodynamic investigation of the redox properties of ceria-titania mixed oxides. *Appl Catal A: Gen*. 2008;335:153–158.
35. Baldychev I, Vohs JM, Gorte RJ. The effect of the thermodynamic properties of zirconia supported Fe_3O_4 on water-gas shift activity. *Appl Catal A: Gen*. 2009;356:225–230.
36. Fogler HS. *Elements of Chemical Reaction Engineering*, 3rd ed. New Delhi: Prentice Hall of India, 2005.
37. Haye RE, Colaczkowski ST, Li PKC, Awdry LS. The palladium catalyzed oxidation of methane: reaction kinetics and the effect of diffusion barrier. *Chem Eng Sci*. 2001;56:4815–4835.
38. ErtlG, Knozinger H, Schuth F, Weitkamp J., editors. *Handbook of Heterogeneous Catalysis*, 2nd ed. Weinheim: Wiley-VCH, Inc., 2008.
39. Dry RE, Shingles T, Boshoff LJ. Rate of the Fischer-Tropsch reaction over iron catalysts. *J Catal*. 1972;25:99–104.
40. Grenoble DC, Estadt MM. The chemistry and catalysis of the water gas shift reaction: the kinetics over supported metal catalysts. *J Catal*. 1981;67:90–102.
41. Amenomiya Y, Pleizier G. Alkali-promoted alumina catalysts. II. Water-gas shift reaction. *J Catal*. 1982;76:345–353.
42. Hou P, Meeker D, Wise H. Kinetic studies with a sulfur-tolerant water gas shift catalyst. *J Catal*. 2003;80:280–285.
43. Hla SS, Park D, Duffy GJ, Edwards JH, Roberts DG, Ilyushechkin A, Morpeth LD, Nguyen T. Kinetics of high-temperature water-gas shift reaction over two iron-based commercial catalysts using simulated coal-derived syn gases. *Chem Eng J*. 2009;146:148–154.
44. Ayastuy JL, Gutierrez-Ortiz MA, Gonzalez-Marcos JA, Aranzabal A, Gonzalez-Velasco JR. Optimization of inlet temperature for deactivating LTWGS reactor performance. *AIChE J*. 2005;51:2016–2023.
45. Radhakrishnan R, Willigan RR, Dardas Z, Vanderspurt TH. Water gas shift activity and kinetics of Pt/Re catalysts supported on ceria-zirconia oxides. *Appl Catal B: Environ*. 2006;66:23–28.
46. Xu J, Froment GF. Methane steam reforming, methanation and water-gas shift. I. Intrinsic kinetics. *AIChE J*. 1989;35:88–96.
47. Bradford BW. Water-gas reaction in low pressure explosions. *J Chem Soc*.1933:1557–1563.
48. Bustamante F, Enick RM. Uncatalyzed and wall-catalyzed foreward water gas shift reaction kinetics. *AIChE J*. 2005;51:1440–1454.
49. TrovarelliA, editor. *Catalysis by Ceria and Related Materials*. London: Imperial College Press, 2002.
50. Jacobs G, Davis BH. Low temperature water-gas shift: applications of modified SSITKA-DRIFTS method under conditions of H_2 cofeeding over metal/ceria and related oxides. *Appl Catal A: Gen*. 2007;33:192–201.
51. Hulburt HM, Srinivasan CD. Design of experiments on the kinetics of the water-gas shift reaction. *AIChE J*. 1961;7:143–147.
52. Kubsh JE, Dumesic JA. In situ gravimetric studies of the regenerative mechanism of water-gas shift over magnetite: equilibrium and kinetic measurements in CO_2/CO and H_2O/H_2 gas mixtures. *AIChE J*. 1982;28:793–800.
53. Azzam KG, Babich IV, Seshan K, Lefferts L. Bifunctional catalysts for single-stage water-gas shift reaction in fuel cell applications. I. Effect of the support on the reaction sequence. *J Catal*. 2007;251:153–162.
54. Azzam KG, Babich IV, Seshan K, Lefferts L. A bifunctional catalyst for the single-stage water-gas shift reaction in fuel cell applications. II. Roles of the support and promoter on catalyst activity and stability. *J Catal*. 2007;251:163–171.
55. Granger P, Lecomte JJ, Leclercq L, Leclercq G. Modeling study of the temperature-programmed conversion curves of NO reduction by CO over supported Pt- and Rh-based catalysts. *Top Catal*. 2001;16/17:349-354.
56. Henry CR, Chapon C, Duriz C. Adsorption-desorption kinetics on epitaxially oriented palladium clusters. *Z Phys D: At, Mol Clusters*. 1991;19:347–351.
57. Verheij LK, Lux J, Anton AB, Poelsema B, Comsa G. A molecular beam study of the interaction of CO molecules with a Pt(111) surface using pulse shape analysis. *Surf Sci*. 1987;182:390–410.
58. Sexton BA, Hughes AE. A comparison of weak molecular adsorption of organic molecules on clean copper and platinum surfaces. *Surf Sci*. 1984;140:227–248.
59. Yeung CMY, Meunier F, Burch R, Thompsett D, Tsang SC. Comparison of new microemulsion prepared "Pt-in-Ceria" catalyst with conventional "Pt-on-Ceria" catalyst for water-gas shift reaction. *J Phys Chem B*. 2006;110:8540–8543.
60. Duarte de Farias AM, Bargiela P, Rocha MGC, Fraga MA. Vanadium-promoted Pt/CeO2 catalyst for water-gas shift reaction. *J Catal*. 2008;260:93–102.
61. González ID, Navarro RM, lvarez-Galván MCA, Rosa F, Fierro JLG. Performance enhancement in the water-gas shift reaction of platinum deposited over a cerium-modified TiO_2 support. *Catal Commun*. 2008;9:1759–1765.
62. Phatak AA, Koryabkina N, Rai S, Ratts JL, Ruettinger W, Farrauto RJ, Blau GE, Delgass WN, Ribeiro FH. Kinetics of the water-gas shift reaction on Pt catalysts supported on alumina and ceria. *Catal Today*. 2007;123:224–234.
63. Zhdanov VP. Some aspects of the kinetics of hydrogen-oxygen reaction over the Pt (111) surface. *Surf Sci*. 1986;169:1–13.

Manuscript received May 5, 2009, and revision received July 7, 2009.